JOURNAL OF CATALYSIS 89, 226–243 (1984)

$Co/Mo/Al_2O_3$ Catalyst Structure Determination by EXAFS

I. Mo K Edge in the Oxidized State

N.-S. CHIU, S. H. BAUER, AND MARVIN F. L. JOHNSON*

*Department of Chemistry, Cornell University, Ithaca, New York 14853 and *ARCO Petroleum Products Company, Harvey Technical Center, Harvey, Illinois 60426*

Received February 14, 1984; revised April 30, 1984

Application of an improved successive approximation data reduction program to EXAFS spectra of a series of unsulfided experimental hydrodesulfurization catalysts showed that when the Mo loading increased, the *apparent* coordination number about the molybdenums decreased; this is indicative of major distortions of the MoO_6 octahedra. Confirmatory evidence was obtained from the near-edge absorption functions which were resolved into three overlapping Gaussians, one of which corresponds (nominally) to the $1s \rightarrow 5p$ transition. Its area, which is also a measure of departure of the coordination shell from a regular octahedron, increased with percentage Mo, a trend which parallels the decrease in the *apparent* coordination number. The addition of Co to these Mo/Al_2O_3 preparations led to a decrease in distortion, as measured by each of these independent indices.

INTRODUCTION

The atomic configurations at the active sites of one of the most extensively used catalysts in the petroleum industry are still unknown. The compositional and chemical properties of hydrodesulfurization catalysts have been thoroughly investigated, and their catalytic effectiveness correlated with established protocols for their preparation, so as to optimize conversions and extend their lifetimes. Yet, there is still considerable debate regarding the physical and chemical features which are directly involved in the mechanism for the extraction of sulfur atoms from the large variety of organic substrates present in feedstocks, and their conversion to H_2S. Characterization by surface areas and pore size distributions at best constitute boundary conditions for any proposed structural model. Because the essential ingredients (Co/Mo or Ni/Mo) are present as amorphous structures on high-area supports, large-angle X-ray diffraction data provide no useful information. Physical methods do show promise for demonstrating the presence of identifiable moieties within a surface layer of a few atomic dimensions; these are Raman, infrared, X-ray photoelectron spectra, and electron energy loss spectra. In addition, Mössbauer and extended X-ray absorption-edge fine structure spectra provide bulk structural information (*1*). At this stage the conclusions derived from the variety of probes are not entirely consistent; this raises questions regarding the uniqueness of the interpretations of the respective data.

Examination of many published Fourier transforms derived from EXAFS spectra suggest that important information may be lost due to the high noise levels. While the locations of the radial distribution peaks are quantitatively significant, their areas which should provide measures of atomic density are unreliable and thus lead to misinterpretations of structural configurations. Due to the complexity of the interatomic scattering process for photoejected electrons, both the distance and amplitude scales of the radial distribution functions deduced from EXAFS must be calibrated by recording

0021-9517/84 $3.00
Copyright © 1984 by Academic Press, Inc.
All rights of reproduction in any form reserved.

spectra of known structures, similar to the ones under investigation. Empirically, it was found that when in the *calibrating* structures the distances between the central (probed) atom and the atoms in the selected coordination shell are uniform, the *deduced* coordination numbers are generally low for structures wherein the distances are substantially nonuniform (*NUD#*) due to local distortions. This is a severe limitation on the utility of EXAFS data, since their principal application is precisely to those amorphous systems which are characterized by structural disorder. We developed an EXAFS data reduction routine which leads to radial distribution curves with substantially lower background noise and high reproducibility in the fwhm of the major peaks. The improved routine was applied to the analysis of absorption spectra at the Mo *K* edges of eight calibrating compounds of molybdenum and a range of Mo–Co/Al_2O_3 hydrodesulfurization catalysts. In this report we describe the oxidic, *precatalyst* stage; structures derived for the H_2S/H_2 reduced sulfided, catalytically active preparations, and their complete characterization will be presented in succeeding reports.

The basic equations for deriving radial distribution curves from EXAFS are summarized in Section I. In Section II our experiments are briefly described. Section III is devoted to a summary of typical near-edge Mo *K* spectra of the nonproprietary catalysts prepared for this investigation. Structural information on MoO_x units in the alumina-supported Mo/Co oxides, derived from the extended absorption coefficients, is presented in Section IV. In another report we have explored the basis for nonadditivity in conventionally derived radial distribution curves, and presented an outline of an improved procedure for data reduction in which the nonadditivity feature has been *minimized but not eliminated.*

SECTION I: BASIC EQUATIONS

The complete theoretical expression for the back-scattered contribution to the post-edge X-ray absorption cross section of an atom surrounded by several coordination shells is elaborate, and incorporates terms which can be computed only approximately (*2*). In contrast, the generally used expression for the reduced absorption coefficient over the extended portion of the *K* edge is sufficiently condensed to permit ready transfer of empirically deduced parameters from known (calibrating) to unknown but closely similar structures (*3*).

$$\chi(k) \equiv \frac{\Delta\mu}{\mu_{BK}} = -\sum_j \frac{N_j}{R_j^2} e^{-2R_j/\Lambda_j(k)} \frac{1}{k} |f_j(k;\pi)| e^{-2\sigma_j^2 k^2} \sin[2kR_j + \psi_j(k)] \quad (1)$$

$\Delta\mu$ is the oscillatory, structure sensitive contribution superposed on the smooth (atomic) background μ_{BK}; N_j is the number of back-scattering atoms in the jth coordination shell; R_j, their distance from the central atom; Λ_j, the internal absorption length for the scattered electrons; σ_j, the Debye–Waller factor; Ψ_j, the phase shift upon scattering, and $|f_j|$ the atom-form factor. In order to deduce radial distribution-like functions from recorded data further simplifications must be introduced. By collecting most of the k-dependent terms into the left member, and replacing the sum over equivalent back-scattering atoms by a continuous distribution function, Eq. (1) can be rewritten in the form

$$\frac{k \cdot \chi(k)}{\langle |f_j(k;\pi)| \rangle} e^{+2\langle\sigma_j\rangle^2 k^2} = \int_0^\infty dR \cdot \frac{D(R)}{R^2} e^{-2R/\langle\Lambda_j\rangle} \sin[2k(R - B) + A] \quad (2)$$

where mean values were introduced for the atomic scattering factors. The left member of this equation is then replaced by $k^3(\Delta\mu/\mu_{BK})$, because it is implied (though not explicitly stated) that for many atom pairs $\langle |f_j(k;\pi)| \rangle \cdot e^{-2\langle\sigma_j\rangle^2 k^2}$ varies approximately as k^{-2}. [Cramer *et al.* (*4*) proposed a more extended parameter-fitting calibration scheme.] The Fourier transform of the function $k^3(\Delta\mu/\mu_{BK})$ is $\rho_1(R_\psi)$ which, when corrected programatically for false background ($\rightarrow\rho_2$), and termination errors

($\rightarrow\rho_3$), and then adjusted empirically for the displacement of scale, approximates the desired radial distribution function, $D(R) \Rightarrow R^2 \cdot \rho_3(R_\psi + B) \cdot \exp(+2R/\langle\Lambda\rangle)$.

While the above procedure leads to reliable values for the mean distances between the central atom and the first, second, and (sometimes) the third coordination shells, the deduced coordination numbers (i.e., the areas under the peaks in the radial functions) may not scale correctly. Eisenberger and Brown (*5*) and particularly Brown (*6*) called attention to this aspect. It is usually stated that nonadditivity of pair contributions is due to loss of data for the low ($0 < k < 4$) and high values of k ($k > 16$). When $D(R)$ in Eq. (2) is smeared, the resulting function in k damps more rapidly than when it peaks sharply at a few values. However, this is not a cogent explanation. In Fourier transforms the *resolution* is limited by the range of integration, as when it is modulated by a rectangular window or an exponential decay, but this can be corrected (*via* an appropriate convergence technique); then the additivity property is retained. Empirically this has been demonstrated innumerable times in the deduction of molecular structures from gas-phase electron diffraction data (*7*).

SECTION II: EXPERIMENTS

EXAFS data obtained at the CHESS (Cornell High-Energy Synchrotron Source) Facility for a representative group of CoO/MoO_3 preparations, deposited on high-area aluminas were reduced according to procedures outlined in Section IV (*8*). The compositions listed in Table 1 were prepared by impregnating extruded Catapal alumina (289 m^2/g), which was first calcined at 823°K, with ammonium molybdate solutions, by the incipient wetness technique; then calcined at 823°K, to give preparations having 2, 4, 6, 12, 18, 24, and 30% MoO_3. In turn, portions of most of these were reimpregnated with cobalt nitrate solution (and after another calcination) to yield catalysts with 1.5, 3.0, 6.0, and 12.0% CoO. A second series was prepared the same way, using a γ-Al_2O_3 with a surface area 194 m^2/g, to determine the effect of a lower area support. These were not reimpregnated with $Co(NO_3)_2$.

TABLE 1

Compositions of Catalysts Investigated via EXAFS (Nominal Percentages, on Catapal)

CoO (%)	MoO_3 (%)							
	2	4	6	12	18	24	30	100
0	X	X	X	X	X	X	X	X
1.5			X	X	X	X	X	
3			X	X	X	X	X	
6			X	X	X		X	
12				X	X			

Note. Also: Commercial catalysts [14.4%/2.7%], and three preparations on a lower area base. Calibrating compounds: from commercial or friendly scientists; used as received.

Two commercially available Co/Mo/γ-Al_2O_3 catalysts were studied, in addition to the one above. One was virgin Nalcomo 477, and the other was a catalyst with the same designation which had seen extensive service in a commercial HDS unit, followed by a careful laboratory regeneration.

The various preparations were fully characterized, and will be described in detail in a forthcoming report. Briefly, the changes in surface area and pore volume, as the MoO_3 was added, were about what one would predict by dilution of the alumina with MoO_3. The pore sizes were not radically reduced, and there was no apparent pore blockage. These results and X-ray diffraction data are consistent with the model in which MoO_3 is deposited as a monolayer on the surface of the alumina. The addition of CoO behaved as an equal quantity of MoO_3. The only discernible large-angle X-ray diffraction peaks were those of the aluminas. Reflectance spectra show that the intensity of the peak at 17,200 cm^{-1}, due to octahedral Co(+2), is not only a function of percentage of Co, as is to be expected, but also a function of percentage of MoO_3 at 1.5–3% CoO. This is an indication of inter-

action between the cobalt and molybdenum oxides.

At the Mo *K* edge all spectra were recorded in the transmission mode. In order to eliminate changes in intensity due to sample inhomogeneities, the samples were ground to pass a 180-mesh sieve. They were then packed into plastic sample holders of selected thickness, with a packing density of about 0.7 to 1.0. The thickness was chosen such that the product of the total absorption coefficient and the holder thickness was approximately 2.5 on the high-absorption side of the edge. Mylar (1 mil) was used for the windows. Monochromaticity was obtained with a channel-cut Si(220) monochromator which was detuned to minimize the harmonic content. The energy spread was due primarily to beam divergence, which could be partially controlled by the width of the final slit (0.5 mm). The beam shape could be approximated by a Gaussian with a *fwhm* of about 6 $\rightarrow$ 12 eV (for a slit width of (0.5 $\rightarrow$ 1 mm) (*9*). The monitoring counter was calibrated relative to the recording counter for each beam fill, as a function of energy, at low counting rates to minimize lost counts due to limited counter recovery time. The absorption spectra were recorded by sequential stepping of the crystal angle, for 1-eV intervals at the *K* edge and for 3-eV intervals for energies from about 40 eV beyond the edge, when the monitoring counter had accumulated a specified preset count ($10^4 \sim 10^5$). A scan of Mo metal foil was taken at the beginning and toward the end of each fill for calibration of the monochromator. The photon flux at Mo *K* edge was about 10^8 photon/sec on exit from the monochromator.

SECTION III: NEAR-EDGE FEATURES

The spectral resolution available at the C_2 station at CHESS allowed us to record characteristic features due to molybdenum ions in a variety of known crystal field environments. These included: (a) regular tetrahedral symmetry [K_2MoO_4]; (b) regular octahedral symmetry [Ba_2CaMoO_6; MoS_2; Mo metal]; (c) a range of distorted octahedra, including a mixed octahedral/tetrahedral case [$(NH_4)_2Mo_2O_7$]. Typical near-edge absorption curves for MoO_x units are illustrated in Fig. 1. The spectra of all the model compounds, except of Ba_2CaMoO_6, MoS_2, and Mo (metal), show a weak peak (or a shoulder) on the low-energy side of the edge. An interval of 50–60 eV which incorporates this portion of the scan was resolved into three Gaussians by least-square fitting of nine parameters. Prior to deconvolution, all $\{\mu(E) \cdot x\}$ values were normalized by dividing them by the magnitude of the total jump from zero level to the background level extrapolated from the high-energy side (μ^*_{BK}). Although the convergence was sensitive to the voltage range allocated to each of the Gaussians, the position of the first peak remained unchanged, and the positions of the other two peaks varied only by ± 1 eV. Furthermore, the relative areas under the three Gaussians were not affected by the assigned voltage ranges. [Of course, resolution into four Gaussians gave better fits, and moved the third peak toward lower energies, generally by 3–6 eV.] The near-edge absorption curves were also deconvoluted into three Lorentzians. The locations of the three maxima were the same as for the Gaussians, generally within 1 eV, but the overall fit was considerably less satisfactory. Table 2 is a summary of the peak positions and areas derived from three resolved Gaussians; each incorporates the apparatus transmission function which is presumed to be Gaussian.

The simplest interpretation of the resolved components of the near-edge spectra is based on the pseudoatomic model (*10*); the assignment sequence is $1s \rightarrow 4d$; $1s \rightarrow 5s$; $1s \rightarrow 5p$. In a tetrahedral field the first transition is allowed, but it is forbidden in a strictly octahedral field. This selection rule breaks down when the octahedra are distorted. The extent of distortion of the octahedron of oxygen atoms in the first coordination shell in the calibrating compounds is measured by

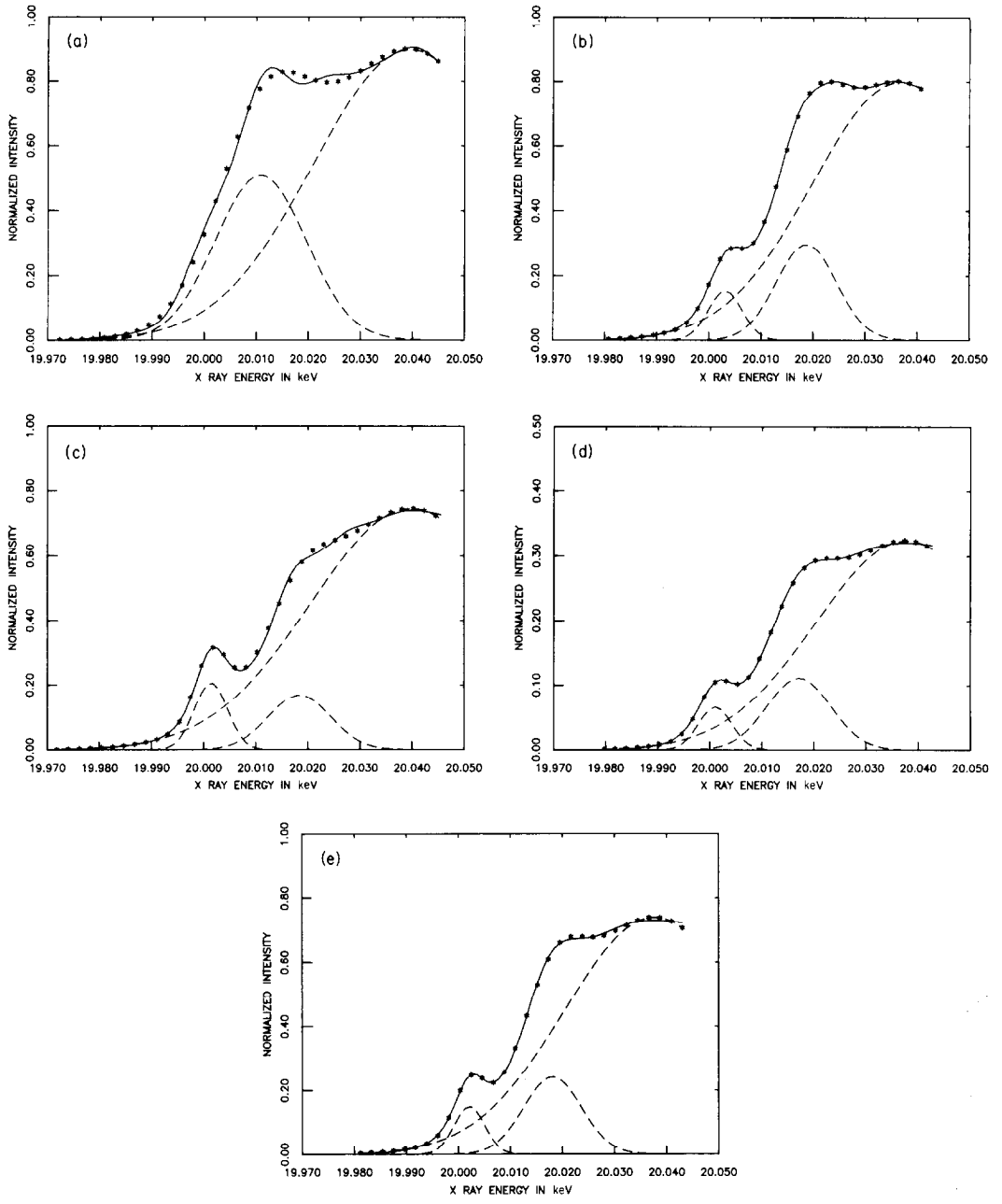

FIG. 1. Resolved near-edge (K) spectra for Mo in three calibrating compounds, and for typical catalyst preparations: (a) Mo metal; (b) MoO_3(cryst); (c) K_2MoO_4; (d) 2% MoO_3 (0% CoO); (e) 18% MoO_3 + 6% CoO, all on Catapal.

$$NUD\# \equiv \frac{1}{p}\sum_{i=1}^{p}\left|\frac{R_i - R_m}{R_m}\right| \qquad (3)$$

where R_m is the arithmetic mean of the Mo–O distances. Inspection of Table 2 suggests that the $NUD\#$ correlates with the magnitude of A_1 but not with A_2. Possibly a measure of the angular distortion (i.e., the direction of the hybrid orbitals) must also be included; i.e.,

TABLE 2

Summary of Parameters of Resolved Gaussians—Near Edge

Compounds	V_1[a]	V_2	V_3	A_1[b]	A_2[b]	A_3[b]	*NUD#*/Comments	
Mo (metal)	—	20,010.7	20,039.3	—	107	411		bcc
K_2MoO_4 (*24*)	20,001.4	20,018.4	20,039.7	16	25	360	0	tetrahedra
$Mo_2O_7^{2-}$ (*17*)	2.7	19.0	40.9	16	45	376	0.094	Mixed: tet : oct
Ba_2CaMoO_6 (*23*)	—	17.1	33.4	—	8	155	0	Reg. oct
Di-bu-at (*22*)	1.2	15.7	31.4	8	27	346	0.070	Dist. oct
$Mo_7O_{24}^{6-}$ (*18*)	3.0	17.8	34.4	12	30	320	0.085	Dist. oct
MoO_3 (*19*)	3.1	18.8	37.4	13	46	344	0.105	Dist. oct
$Mo_2O_5(PQ)_2$ (*20*)	2.3	16.2	32.5	14	29	353	0.125	Dist. oct
Catalysts MoO_3/CoO								
2/0	20,001.0	20,017.1	20,037.7	5	17	141		
4/0	2.5	18.7	38.9	8	24	212		
6/0	2.2	18.2	38.7	10	27	259		
12/0	2.1	18.0	37.7	11	34	317		
18/0	2.3	18.2	37.8	12	40	348		
24/0	3.2	19.2	38.8	12	41	357		
30/0	2.9	18.9	37.9	12	40	355		
6/1.5	2.0	18.2	38.7	9	25	246		
6/3.0	2.3	18.3	38.0	8	24	229		
6/6.0	1.9	18.2	38.6	8	22	209		
12/1.5	2.1	18.2	38.0	11	34	306		
12/3.0	2.0	18.0	37.8	10	30	297		
12/6.0	3.0	19.2	39.1	10	31	277		
12/12.0	2.1	18.2	38.2	9	27	244		
14.4/2.7	2.1	17.8	37.0	11	31	299	[c]	
14.4/2.7	2.4	17.9	36.3	9	28	260	[d]	
18/1.5	2.3	17.8	37.0	11	39	336		
18/3.0	2.1	18.0	37.6	11	36	332		
18/6.0	2.1	18.0	37.7	11	33	316		
18/12.0	2.0	18.4	39.1	11	35	306		
24/1.5	2.4	18.4	37.7	12	40	353		
24/3.0	2.2	18.2	37.6	12	39	348		
30/1.5	2.5	18.4	37.4	12	41	361		
30/3.0	2.5	18.6	38.1	12	40	356		
30/6.0	2.2	18.6	39.0	13	41	355		
12/0	2.3	18.2	38.1	10	34	313	Lower area support	
18/0	2.5	17.9	36.5	11	35	329	Lower area support	
24/0	2.6	17.7	36.2	12	36	342	Lower area support	

[a] All voltage readings were corrected with reference to their midpoints at the *K*-edge jumps, referred to Mo(metal) at 20,002.0 eV.

[b] Areas are in a consistent set of (arbitrary) units for *normalized* absorption curves.

[c] Commercial sample.

[d] Commercial sample (regenerated), see text.

$$NUA\# \equiv \frac{1}{q_{(ij)}} \sum^{q} \left| \frac{\theta_{ij} - \pi/2}{\pi/2} \right| \quad (4)$$

Of special interest in the study of hydrodesulfurization catalysts is the clear dependence on composition of the magnitudes of A_1; A_2; A_3 (interpreted as measures of transition probabilities for the corresponding transitions), while the values V_1; V_2; V_3 remain essentially unchanged. $A_1 = 16$ for MoO_4^{2-} and $Mo_2O_7^{2-}$; this high value may be used as a measure of tetrahedral content. Also note A_1, and to a more marked extent A_3, which increase with MoO_3 loading but decrease (for a constant Mo) with CoO loading (Table 2 and Fig. 2). This correlation holds approximately for externally prepared samples as well. The commercial virgin 14.4/2.7 sample is close to our 12/3 preparation. Regeneration induced a reduction in the peak areas. We propose that the magnitudes of these areas measure the degree of distortion of the octahedral unit, suggesting that the effect of the promoter is to reduce distortion for a given Mo loading; regeneration has a similar effect. The sensitivity to CoO decreases with increasing MoO_3 loading, as expected when the monolayer is crowded.

Asada (*11*) claims that the oxidation number of the metal atom, rather than the coordination number determines the presence of the first weak absorption. For metals, Grunes (*12*) found excellent agreement between one-electron calculations and the observed *K*-edge spectra, but for metal oxides, that formulation was not "auspicious." A review of X-ray absorption-edge spectrometry, with reference to coordination problems, was prepared by Srivastava and Nigam (*13*). Seka and Hanson (*14*) presented the initial molecular-orbital interpretation of X-ray absorption-edge structures. In MoO_4^{2-}, Kutzler *et al.* (*15*) showed, on the basis of SCF-Xα calculations, that the first relatively intense peak

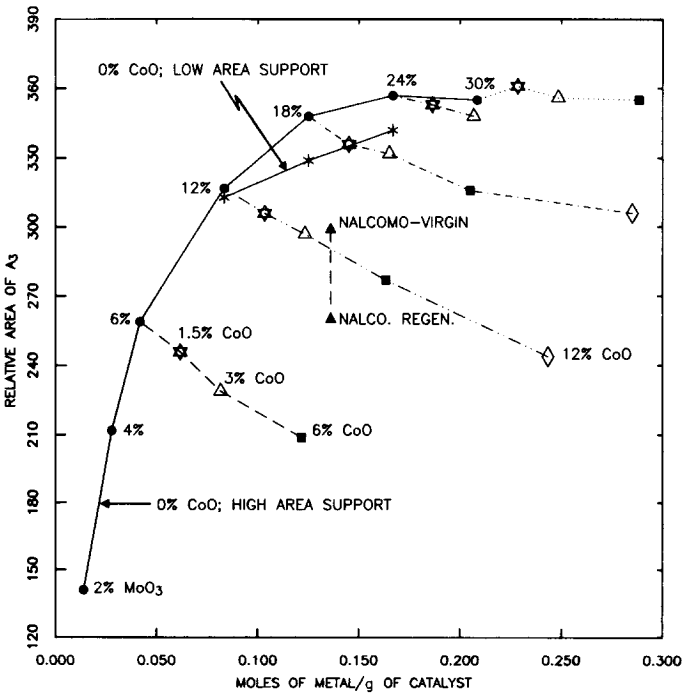

FIG. 2. The dependence of A_3 (nominally assigned to the $1s \rightarrow 5p$ transition) on the MoO_3 and CoO content of the catalyst preparations (Table 2). (●) 0% CoO; (✡) 1.5% CoO; (△) 3% CoO; (■) 6% CoO; (◇) 12% CoO; (*) 0% CoO on lower area support; (▲) Nalcomo.

is due to a bound anti-bonding state which is mainly 4*d* in character; that the shoulder on the rising portion of the absorption curve can be described as the beginning of a step-like continuum absorption, while the main absorption peak is due to a dipole-allowed transition to a continuum state of T_2 symmetry.

The edge *position* is clearly dependent on the oxidation state of the metal atom (*16*). The edges of the catalysts were found to lie within a range of 2 eV (7.5–9.4 eV from Mo metal), while in the reference compounds they span the interval 7.0–9.4 eV. In the latter, the oxidation state is +6. Hence we conclude that in the various catalyst preparations, the oxidation state of the molybdenum remains +6, and the small variations in edge position have their origin in small local perturbations. The *K* edges moved toward lower energies when these preparations were reduced by H_2S/H_2. The net shift was about 8 eV, from Mo(VI) in the oxide to Mo(IV) in the sulfide. The edge position is linearly related to the extent of reduction but only during the early periods of reduction.

SECTION IV: EXAFS DATA REDUCTION AND RESULTS

Examination of the many radial functions derived from EXAFS spectra published during the past 5 years convinced us that a considerable improvement could be achieved by (A) "smoothing" of the large number of data points which can be collected at synchrotron sources, to minimize extraneous noise; (B) deconvolution of the spectra to correct for finite energy transmission by the monochromator, and beam divergence; (C) correction for the background absorption (μ_{BL}) due to the underlying wings from the *L* edges of the central species, and wings from other absorbers; (D) imposing an objective criterion for drawing in the background ($\mu_{BK} + \mu_{BL}$); (E) corrections for truncation errors.

These steps (as well as the "conventional" procedures for correcting the energy scale by appropriate selection of V_0, etc.) led to improved radial distribution curves, with lower background noise and enhanced reproducibility of the fwhm's for the major peaks, as can be assessed from Fig. 3(a,b,c;d,e,f). We found that for test samples, such as a series of mechanical mixtures [K_2MoO_4 + Al_2O_3; MoO_3 + Al_2O_3] the peak areas were reproduced to ±5% for dilutions 20 → 75%. Note that while the $D(R)$ curves have much less noise than the conventional one-step reduction, and additionally have a more direct physical interpretation, they still do not fully comply with the additivity property of Fourier transforms, because the *starting function is badly distorted.* Until that inherent perturbation has been removed we propose to use a *calibrating curve,* to obtain estimates of the number of atoms present in close proximity to the central atom. This number we designate the "apparent" coordination (η), which is less than the conventionally defined C.N. The latter counts all the neighbors in the first shell, while the former counts only the nearest neighbors.

Calibration for N_j

To develop an empirical calibration curve for a specified coordination shell it is necessary to record EXAFS spectra for three or four known structures which cover a range of structural disorders; i.e., nonuniformity in bond angles and in distances between the central atom and the atoms which comprise the first coordination shell. Transforms of their $k^n\chi(k)$ functions (following our optimized routine) give radial distribution (R.D.) peaks, from which one can read paired values for the area/atom-pair (A_{MX}) and the fwhm, evaluated by dividing the area by the peak height. [Direct measures of peak widths were found to be inaccurate for cases where the R.D. peaks are partially resolved.] The curve drawn through these points can be used to interpolate magnitudes of A_{MX} for unknown structures, given their *fwhm* values. Then the corresponding η's can be estimated from

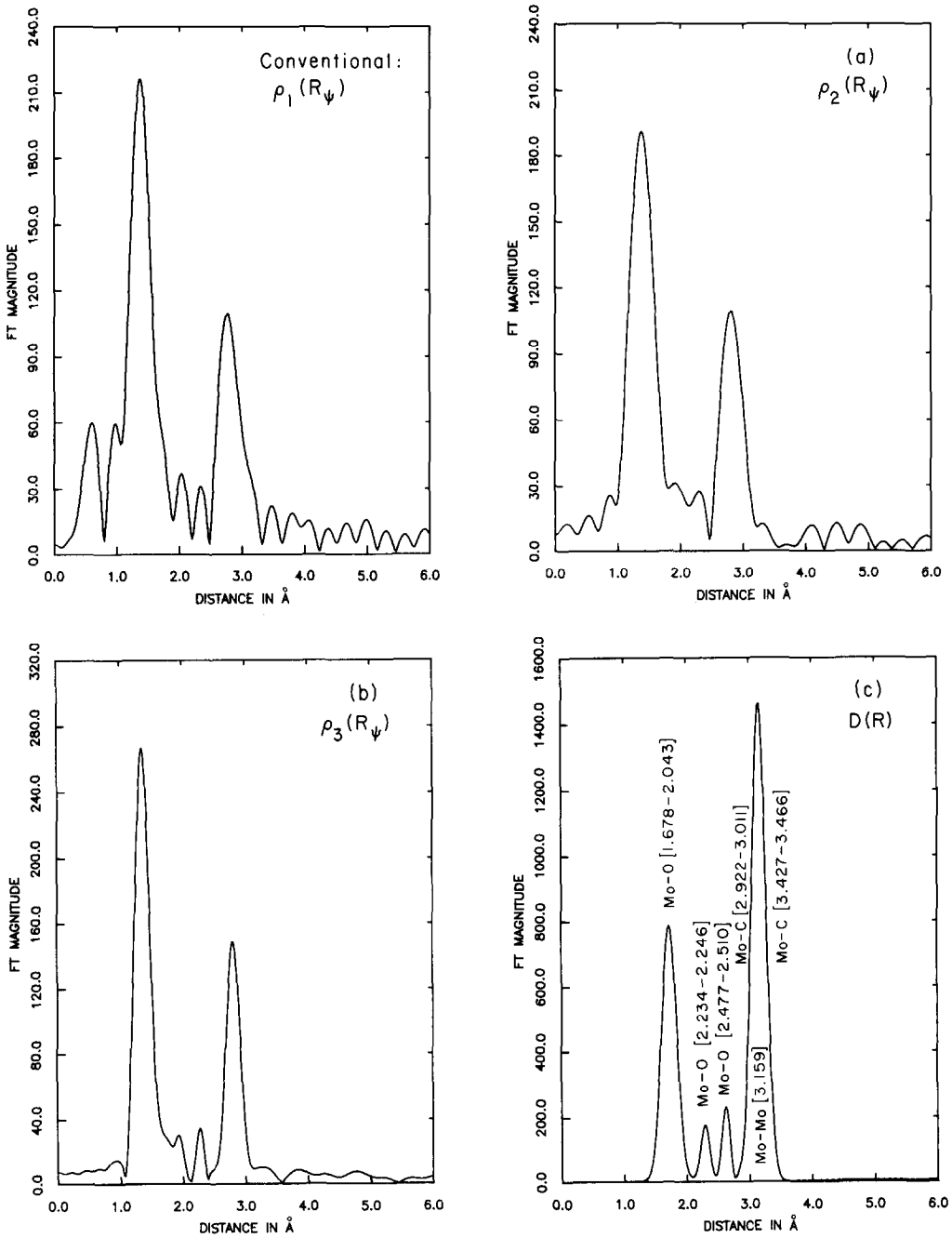

FIG. 3. Successive improvements of the radial distribution functions for $Mo_2O_5[PQ]_2$ (a,b,c) and a catalyst preparation: 12% MoO_3 + 1.5% CoO supported on Al_2O_3 (d,e,f). For each material the panel marked: $\rho_1(R_\psi)$: conventional, is self-explanatory: $\rho_2(R_\psi)$ is the radial function correction for faulty background; $\rho_3(R_\psi)$ results after correction for termination errors; $D(R) = R^2\rho_3(R_\psi + B) \cdot \exp(2R/\langle\Lambda\rangle)$, where B is the phase-shift for the particular atom-pair, and $\langle\Lambda\rangle$, the mean absorption length, was set at a constant value, 3 Å.

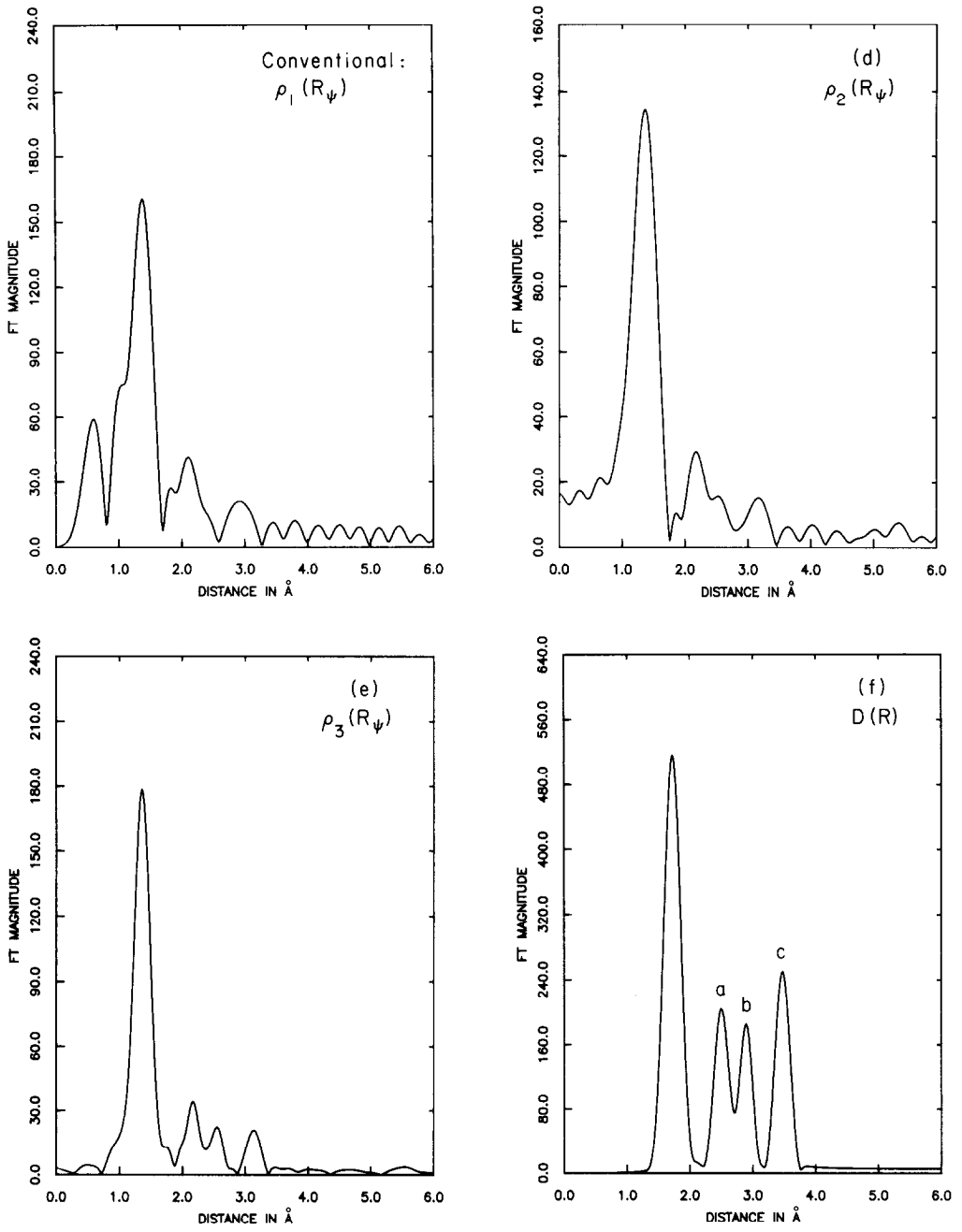

FIG. 3—*Continued.*

the peak areas. Such a calibrating curve for distorted octahedra of MoO_6 is shown in Fig. 4. The following compounds were used: $(NH_4)_2Mo_2O_7$ (*17*); $(NH_4)_6Mo_7O_{24} \cdot 4H_2O$ (*18*); MoO_3 (*19*); $Mo_2O_5(PQ)_2$ (*20*); [PQ ≡ 9,10-phenanthrene quinone] ($Mo(PQ)_3$ has also been synthesized (*21*)); and $[MoO\{O_2C_6H_2(t\text{-bu})_2\}_2]_2$ (*22*). Samples of Ba_2CaMoO_6 (prepared by Dr. Arthur W. Sleight, Du Pont Experimental Station; structure by Steward and Rooksby (*23*)), which is presumed to consist of regular oc-

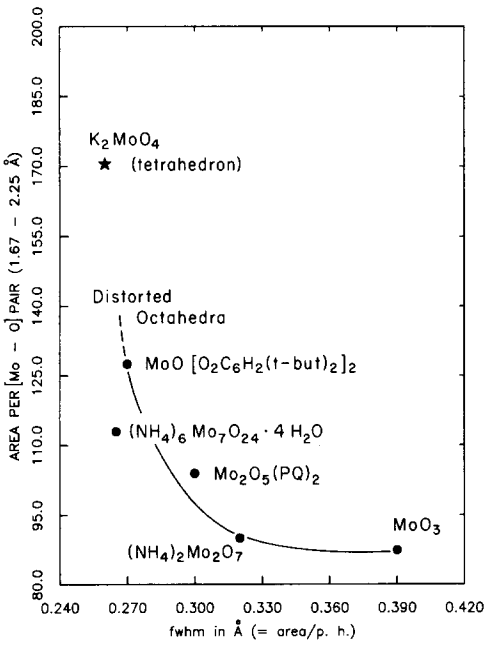

FIG. 4. Calibration curve for the first coordination shell of oxygen atoms around molybdenum.

tahedra, and K_2MoO_4 (*24*), with regular tetrahedra, were also run. Clearly such a calibration is not applicable to cases when an unresolved peak incorporates two types of widely different scattering contributions (MX_n and MY_m), as is the case for $Mo_2(O_2CCH_3)_4$ (*25*), wherein the first peak is a superposition of Mo–Mo and Mo–O terms.

The Radial Distribution Curves

The $D(R)$ curve for MoO_3(cryst) shows a relatively broad first peak, which corresponds to a coordination shell of 6 oxygen atoms in a highly distorted octahedron around the molybdenum (Fig. 5a), a broad second peak for a coordination shell which is comprised of both Mo and O atoms; and a third peak centered at ≈5.5 Å. The $D(R)$ of $(NH_4)_6Mo_7O_{24} \cdot 4H_2O$ is similar but with better resolution, as is the $D(R)$ of $Mo_2O_5[PQ]_2$ (Fig. 3c). In contrast, the oxide catalysts uniformly show a narrow first peak (Figs. 3f;5d,e), with subsidiary smaller peaks at larger R's. The $D(R)$'s of the catalysts confirm the accepted model that the molybdenum atoms are extensively dispersed on the support surface; contrast the relative peak intensities in the catalysts with those in the calibrating compounds.

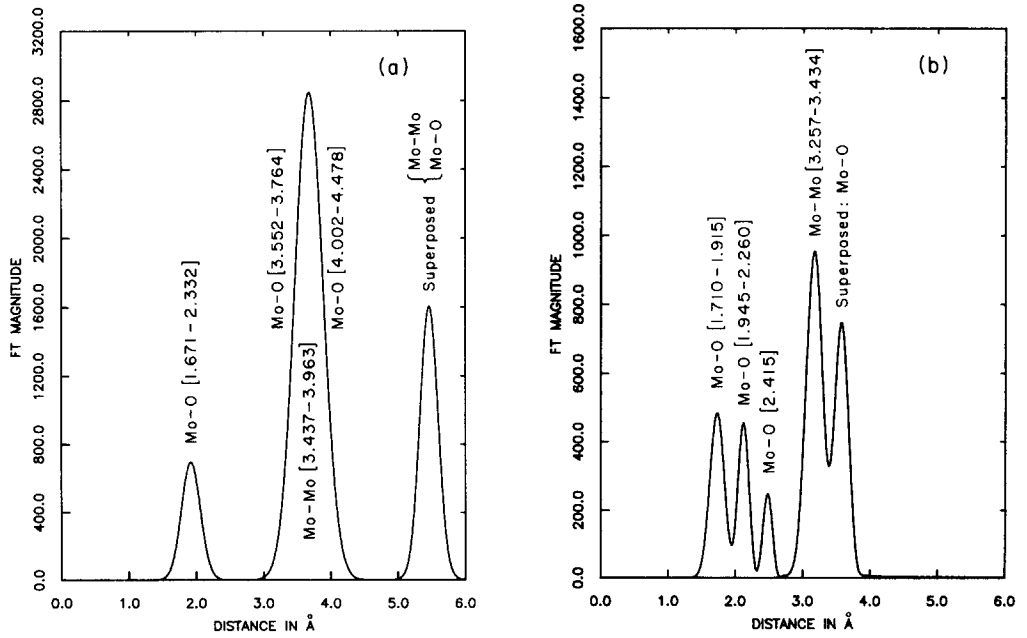

FIG. 5. $D(R)$ curves for (a) crystalline MoO_3; (b) $(NH_4)_6Mo_7O_{24} \cdot 4H_2O$; (c) K_2MoO_4, and three catalyst preparations: (d) 4% MoO_3 + 0% CoO; (e) 30% MoO_3 + 0% CoO; (f) 30% MoO_3 + 1.5% CoO.

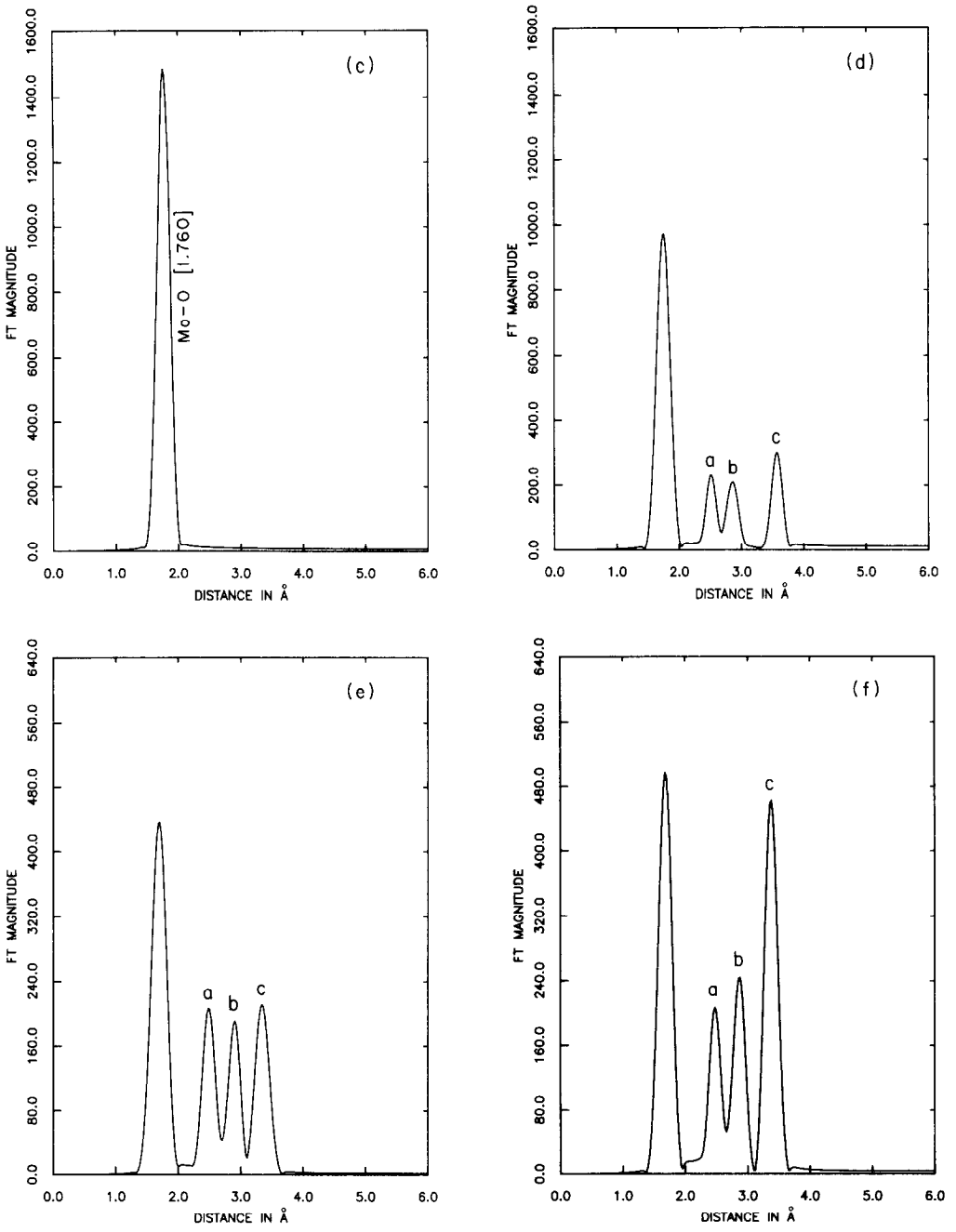

FIG. 5—*Continued.*

[About 30% MoO_3 loading is required to fill a monolayer on a base of this area.] The positions of the primary maxima do change slightly with Mo composition in the expected direction for the high-area support (Fig. 6). For the Mo–O distances represented by the main peak, the mean bond-order (*26*) increases from 1.6 (d = 1.75 Å) to 2.0 (d = 1.69 Å). There is no significant effect on the mean Mo–O distances induced by the CoO promoter, but the three preparations on the low-area support show

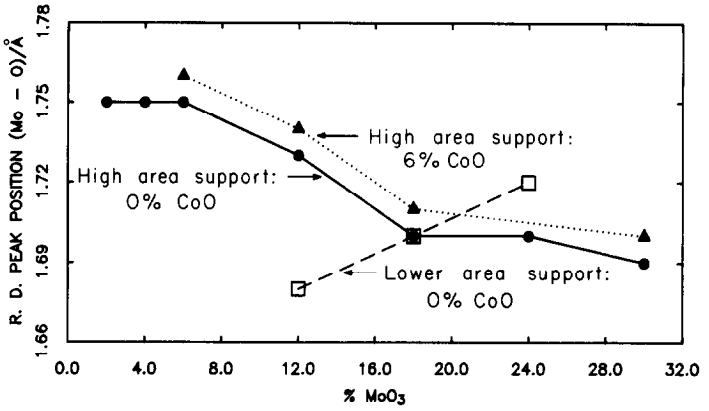

FIG. 6. Dependence of the peak position (*phase corrected*) of the principal Mo–O distance on catalyst composition.

a surprising trend. The narrowing of the radial distribution peaks from ≈0.40 Å for MoO_3 to a fwhm range (0.27–0.33 Å) for the catalysts indicates that crystal packing constraints on the edge-shared octahedra in MoO_3(cryst) were *relaxed* upon dispersal of the oxide over the large surface of the support.

The consequence of MoO_3 loading on the Mo–O peak areas is illustrated in Fig. 7. The preparations on low-area supports almost match the Catapal preparations when they are shifted to higher MoO_3 levels in proportion to their packing densities. The presence of CoO has no measurable effect on the 6% MoO_3 but has clearly discernible

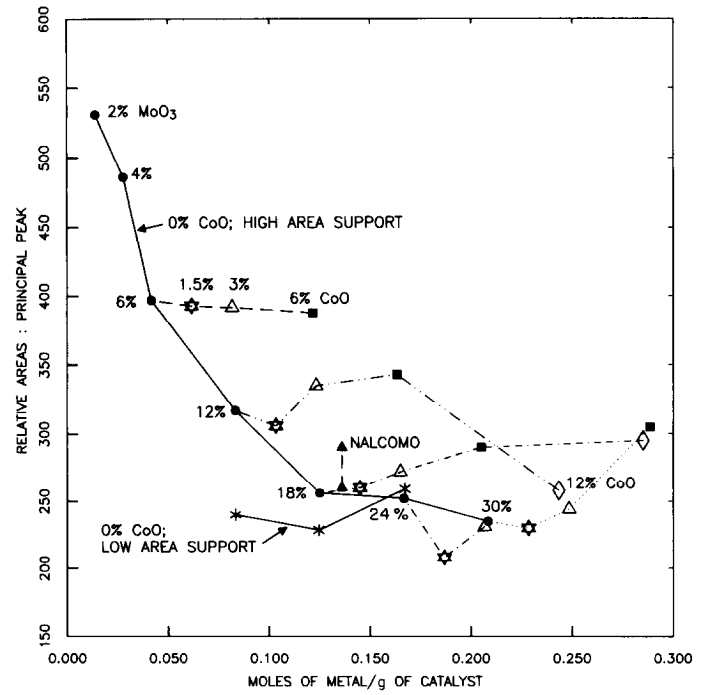

FIG. 7. Dependence of the relative area of the principal peak, for the oxided catalysts, on MoO_3 and CoO content.

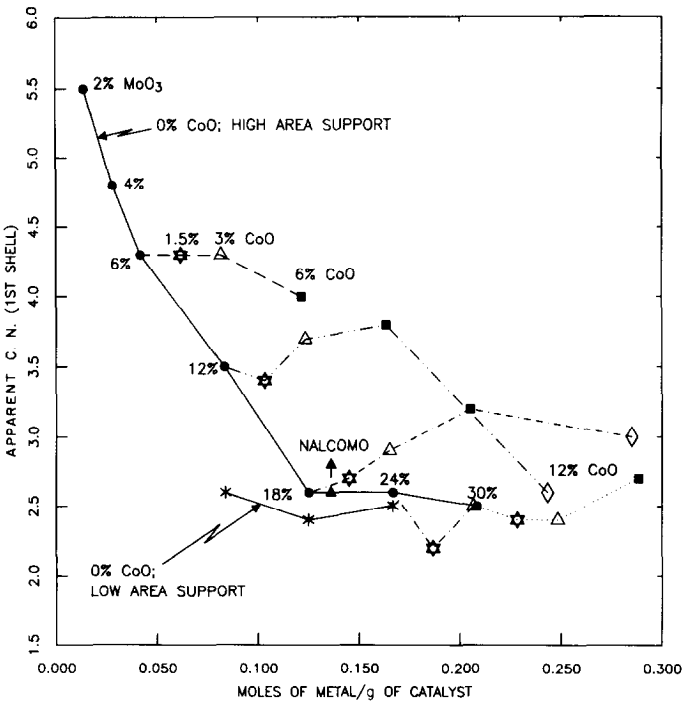

FIG. 8. Apparent coordination numbers (η) deduced from the areas (Fig. 7), based on the calibration curve in Fig. 4.

effects on 12% and higher loadings of MoO_3. These areas were translated into "apparent coordination numbers (η)," on the basis of the calibration curve (Fig. 4), derived from known distorted octahedral and mixed octahedral/tetrahedral MoO_x units, which include a range of *NUD#*. They are plotted in Fig. 8; on this scale the effect of CoO loading is more apparent. The trends parallel those indicated by the A_3 areas in Fig. 2. For 12% MoO_3, the introduction of CoO (1.5–6%) increases the magnitude of η, but a much larger amount of the promoter, such that the total metal content is greatly increased, drastically reduced η. This trend is also shown by 18% MoO_3. CoO has little effect on heavily loaded catalysts (>24% MoO_3). Note that these plots incorporate a correction for some distortion, expressed by the fwhm values. Hence an additional factor is present which further reduces the areas of the major R.D. peaks in the catalyst preparations. One is forced to assume that the highly dispersed molybdenum atoms have η oxygens which are closely bound, and (6-η) which are present over a range of significantly larger distances which are observed but at considerably diminished intensities, due to the R^{-2} weighting of their contributions. The preparations with higher Mo content show lower η's. For the 18–30% level (no CoO) the mean number is ≈2.5. Since about half the oxygens in the extensively dispersed MoO_6's must have originated from the support, it is not unreasonable to postulate that the crowding of the Mo's for these samples forces some of the metal atoms into distorted tetrahedral sites. This is consistent with the low values of A_1 (Table 2) for catalysts with low Mo concentrations (hence indicative of small distortions of the octahedra) and with higher A_1 values for high Mo loading, indicative of high distortions. However, for the catalysts, A_1 does not attain the value 16, characteristic of regular tetrahedra.

The $D(R)$ curves of the oxide catalysts

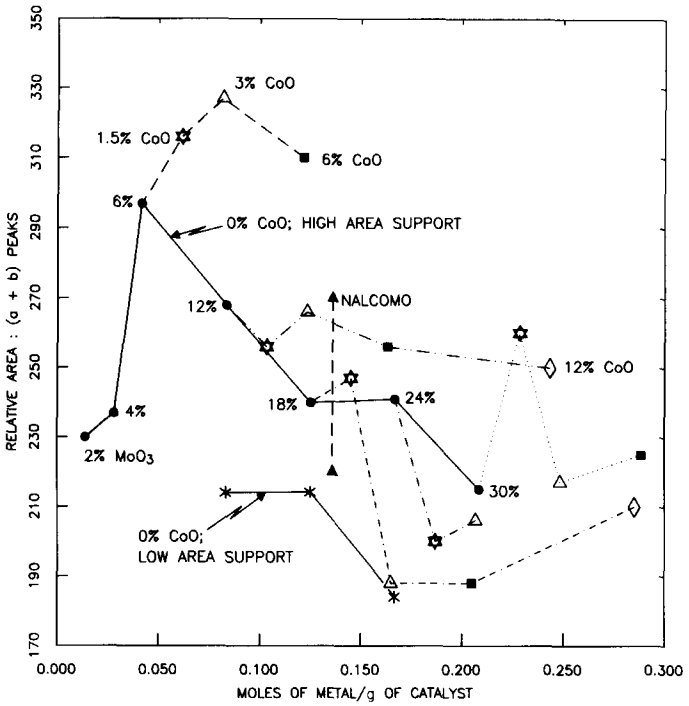

FIG. 9. Dependence of the combined areas of peaks *a* and *b* on catalyst composition.

show three additional peaks; labeled *a*, *b*, and *c* (Figs. 3f; 5d, e). They appear consistently, but due to the R^{-2} weighting, estimation of their areas is less reliable than for the principal peak. Generally *a* and *b* are only partially resolved; they are located at 2.53–2.57 and 2.85–2.87 Å, respectively. Peak *c* appears in the interval 3.35–3.77 Å. Because there are no matching model compounds definite assignments cannot be made, but the possibility that these are due to Mo–Co is eliminated since these peaks appear on all the preparations where no CoO is present. Peak *a* occurs at a distance too short for Mo–Mo or Mo–Al contributions. The only remaining choice is Mo–O. This is consistent with the available structural data; in most of the distorted octahedra in the model compounds there are Mo–O distances as long as 2.5 Å. Indeed, peak *a*, could be part of the MoO_6 octahedron. Peak *b* occurs at about 2.8 Å but the possibility that this is an Mo–Mo distance is discounted (even though such a distance does occur in well-crystallized structures) because the positions of peaks *a* and *b* do not vary with MoO_3 and CoO loading. However, whether peak *b* is due to Mo–Al or to Mo–O, one may argue that both peaks *a* and *b* are associated with the presence of a bond between the molybdenum atoms and the substrate (The range of structural types of molybdenum oxide species mounted on aluminas was summarized by Weigold (*27*)). For 12% MoO_3 the CoO content has little effect on the total area for *a* and *b*. The presence of the promoter increases the (*a* + *b*) area for 6% MoO_3, but decreases it for >18%. The indicated trend with total metal loading (Fig. 9) could be due to increased distortion of the octahedron (see Section II). Again, the points for the low-area support roughly match the higher MoO_3 loadings.

It is likely that peak *c* is due to Mo–Mo; there is a corresponding peak at this distance in MoO_3. It appears that when the Mo loading is increased the trend in the area of

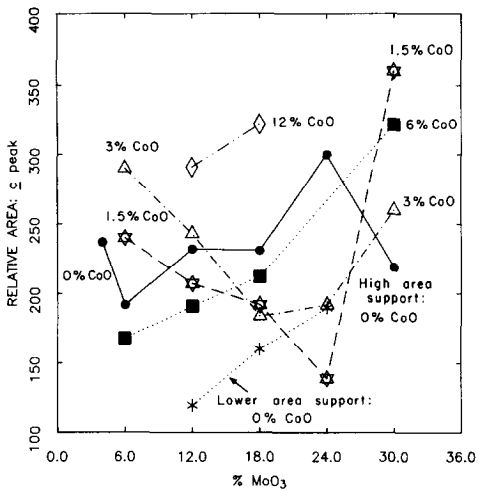

FIG. 10. Dependence of the area of peak c on MoO_3 and CoO composition.

peak c is also toward an increase, and the peak position shifts somewhat to lower R values. When the CoO content is increased the position of peak c is also shifted to lower R's. In 2% MoO_3 with no CoO, there is no c peak. It may have been reduced to the level of the noise. In detail, the relative areas (Fig. 10) are not readily rationalized. Random errors in the data play havoc with this region of the R.D. curves. Note that on comparing the area of the peak assigned to Mo–Mo with the combined areas of the peaks assigned to Mo–O, the relative number of atom pairs is reduced by the ratio of atomic numbers

$$\frac{n(\text{Mo–Mo})}{n(\text{Mo–O})} = \frac{A(\text{Mo–Mo})}{A(\text{Mo–O})} \cdot \frac{Z_O}{Z_{Mo}}.$$

In concluding this section we call attention to the additional information, which can be derived from well-conditioned EXAFS data but is not available when the spectra are reduced following conventional programs. Previous investigators found strong similarities between their radial distribution-like functions for $Na_2MoO_4 \cdot 2H_2O$-type structures and the alumina-supported molybdenum oxides (*28*). All those catalyst preparations looked alike and the presence of the promoter could not be discerned (*29*). The structures of the catalyst preparations which we examined differ markedly from those of the available model compounds, as well as from the published curve for α-$CoMoO_4$. We noted subtle differences between the radial functions, which depend on the molybdenum and cobalt loading. Of particular interest, is the trend shown by the near-edged resolved spectra. However, direct correlation with activity data is to be expected only when similar analyses are completed of EXAFS spectra recorded for the H_2/H_2S-reduced preparations.

SECTION V: DISCUSSION

Attempts to describe and quantitate distorted structures in terms of departures from symmetric figures are unavoidably frustrating. Indeed, in the pertinent literature "disorder" refers both to random packing of structural units, and to geometric distortions of these units. In Section III the terms *NUD#* and *NUA#* were introduced to describe the latter. However, their evaluation is arbitrary when large departures from a regular tetrahedron or octahedron are present.

Of the large variety of probes which have been used to explore the structures of HDS catalysts the most wide ranging appear to be those by Zingg *et al.* (*30*) [ESCA, XPS, ISS, Raman]. There is general agreement that the oxidation number for molybdenum in the oxide state is +6, based on binding energy measurements (*31*) [B.E. (Mo, $3d_{3/2}$) = 232.6 eV; B.E. ($3d_{5/2}$) = 228.6 eV]. Possibly more detailed structural information can be derived from these experiments, and from Mössbauer spectra (*32*) and PAS, regarding the state of the cobalt. However, there are apparent discrepancies between two types of probes which bear directly on the molecular geometry around Mo: Raman vs EXAFS.

Interpretation of vibrational bands in the range 800–1000 cm^{-1} recorded for typical catalyst preparations of alumina-supported Mo and Co oxides, by several groups of

investigators (*33*), indicate the presence of MoO_3 (peaks at 820 and 994 cm^{-1}), at high loadings, and polymolybdate species at low loadings. These spectra suggest that Co hinders the formation of MoO_3 by enhancing dispersion of the Mo. At low coverage the Mo is presumed (*30*) to be in tetrahedral sites, while at higher concentrations both tetrahedral and octahedral units are present. In contrast, the EXAFS data show higher effective coordination numbers for low coverage, and (compared to MoO_3 cryst) relatively little Mo–Mo scattering even at 30% loading. Note the scale factors in Fig. 5a ($\times 10^2$) vs Figs. 5d and e ($\times 10^1$). Significant quantities of two-dimensional polymolybdates are not sampled by EXAFS spectra. The uniqueness of the Raman assignments in terms of tetrahedral vs octahedral units has been called into question (*33f*). Possibly the observed band frequencies are due to local modes rather than to specific structural moieties. The radial distribution functions derived from EXAFS suggest a distribution of distorted geometries which are not readily described in terms of small departures from regular polyhedra.

ACKNOWLEDGMENTS

This work was supported by the National Science Foundation under an Industry/University Cooperative Research Program, Grant CPE-80-00025. The EXAFS spectra were recorded at the Cornell High-Energy Synchrotron Source, supported by NSF Grant DMR-780/267. We thank Dr. Dennis Mills for helpful discussions regarding the estimates of the beam divergence at the CHESS Facility. Also, we acknowledge with thanks, calibrating samples furnished by Dr. A. W. Sleight (DuPont Experimental Station), Dr. G. A. Tsigdinos (Climax Molybdenum), Professor L. Que (Cornell), and Professor F. A. Cotton (Texas A&M). The catalysts were prepared by Mr. R. W. Tumbula (ARCO).

REFERENCES

1. Topsoe, H., *in* "Surface Properties and Catalysis by Non-Metals" (J. P. Bonnelle *et al.*, Ed.). Reidel, Dordrecht, 1983.
2. Teo, B.-K., and Lee, P. A., *J. Amer. Chem. Soc.* **101,** 2815 (1979); Lee, P. A., and Beni, G., *Phys. Rev. B* **15,** 2862 (1977).
3. Lee, P. A. *et al.*, *Rev. Mod. Phys.* **53,** 769 (1981); Gurman, S. J., *J. Mater. Sci.* **17,** 1541 (1982).
4. Cramer, S. P. *et al.*, *J. Amer. Chem. Soc.* **100,** 2748 (1978).
5. Eisenberger, P., and Brown, G. S., *Solid State Commun.* **29,** 481 (1979).
6. Brown, G. S., *in* "Synchrotron Radiation Research" (H. Winick and S. Doniack, Eds.), pp. 392ff. Plenum, New York, 1980.
7. Bauer, S. H., "Physical Chemistry" (H. Eyring *et al.*, Eds.), Vol. 4, Chap. 14, p. 741. Academic Press, New York, 1970.
8. Bauer, S. H., Chiu, N.-S., and Johnson, M. F. L., *J. Mol. Catal.* **20,** 392 (1983).
9. Private communication from CHESS staff—Dr. Dennis M. Mills.
10. Shulman, R. G. *et al.*, *Proc. Nat. Acad. Sci. USA* **73,** 1384 (1976).
11. Asada, E., *Chem. Lett. (Jpn.)* 1467 (1974).
12. Grunes, L. A., *Phys. Rev. B* **27,** 2111 (1983).
13. Srivastava, V. C., and Nigam, H. L., *Coord. Chem. Rev.* **9,** 275 (1972).
14. Seka, W., and Hanson, H. P., *J. Chem. Phys.* **50,** 344 (1969).
15. Kutzler, F. W. *et al.*, *J. Chem. Phys.* **73,** 3274 (1980).
16. Cramer, S. P. *et al.*, *J. Amer. Chem. Soc.* **105,** 799 (1983); **98,** 1287 (1976).
17. Armour, A. W., Drew, M. G. B., and Mitchell, P. C. H., *J. Chem. Soc. Dalton Trans.* 1493 (1975).
18. Evans, H. T., Jr., *J. Amer. Chem. Soc.* **90,** 3275 (1968).
19. Kihlborg, L., *Ark. Kem.* **21,** 357 (1963).
20. Pierpont, C. G., and Buchanan, R. E., *J. Amer. Chem. Soc.* **97,** 6450 (1975).
21. Pierpont, C. G., and Buchanan, R. E., *J. Amer. Chem. Soc.* **97,** 4912 (1975).
22. Buchanan, R. E., and Pierpont, C. G., *Inorg. Chem.* **18,** 1616 (1979).
23. Steward, E. G., and Rooksby, H. P., *Acta Crystallogr.* **4,** 503 (1951).
24. Gatehouse, B. M., and Leverett, P., *J. Chem. Soc. (A)* 849 (1969).
25. Kelly, M. H., and Fink, M., *J. Chem. Phys.* **76,** 1407 (1982).
26. Schroder, F. S., *Acta Crystallogr. Sect. B* **31,** 2294 (1975).
27. Weigold, H., *J. Catal.* **83,** 85 (1983).
28. Parham, T. G., and Merrill, R. P., *J. Catal.* **85,** 295 (1984).
29. Clausen, B. S. *et al.*, *J. Phys. Chem.* **85,** 3868 (1981).
30. Zingg, D. S. *et al.*, *J. Phys. Chem.* **84,** 2898 (1980).
31. Chiu, R. L., and Hercules, D. M., *J. Phys. Chem.* **86,** 3079 (1982); Sarode, P. R. *et al.*—Prepublication report from the laboratory of Professor J. M.

Thomas, Cambridge University; Grimblot, J., Bonnelle, J. P., and Beaufils, J. P., *J. Electron. Spectrosc. Relat. Phenom.* **8,** 437 (1976).

32. Topsøe, H., Clausen, B. S., Candia, R., Wivel, C., and Mørup, S., *J. Catal.* **68,** 433 (1981).

33. (a) Knozinger, H. *et al.*, *J. Phys. Chem.* **84,** 1825 (1980) and previous publications; (b) Dufresne, P. *et al.*, *J. Phys. Chem.* **85,** 2344 (1981); (c) Howe, R. F. *et al.*, *J. Phys. Chem.* **86,** 1233 (1982); (d) Cheng, C.-P., and Schrader, Jr., G. L., 1978 Meeting of the National AIChE (June); (e) Wang, Li, and Hall, W. K., *J. Catal.* **77,** 232 (1982); (f) Schrader, G. L., and Chang, C. P., *J. Catal.* **77,** 232 (1982); *J. Phys. Chem.* **87,** 3675 (1983).